

## Article

# An Effective Joint Soft-Sensing Strategy for Multi-Information under Diverse Vehicle Driving Scenarios

Jianfeng Chen <sup>1</sup>, Jiantian Sun <sup>1</sup>, Shulin Hu <sup>1</sup>, Yicai Ye <sup>1</sup>, Haoqian Huang <sup>2</sup> and Chuanye Tang <sup>1,\*</sup>

<sup>1</sup> Automotive Engineering Research Institute, Jiangsu University, Zhenjiang 212013, China; cjf@ujs.edu.cn (J.C.); jiantiansun@126.com (J.S.); hushulin1158327800@163.com (S.H.); yyc1385098@163.com (Y.Y.)

<sup>2</sup> College of Energy and Electrical Engineering, Hohai University, Nanjing 210098, China; hqhuang@hhu.edu.cn

\* Correspondence: tangchuanye@ujs.edu.cn; Tel.: +86-1886-087-1657

**Abstract:** A variety of accurate information inputs are of great importance for automotive control. In this paper, a novel joint soft-sensing strategy is proposed to obtain multi-information under diverse vehicle driving scenarios. This strategy is realized by an information interaction including three modules: vehicle state estimation, road slope observer and vehicle mass determination. In the first module, a variational Bayesian-based adaptive cubature Kalman filter is employed to estimate the vehicle states with the time-variant noise interference. Under the assumption of road continuity, a slope prediction model is proposed to reduce the time delay of the road slope observation. Meanwhile, a fast response nonlinear cubic observer is introduced to design the road slope module. On the basis of the vehicle states and road slope information, the vehicle mass is determined by a forgetting-factor recursive least square algorithm. In the experiments, a contrasted strategy is introduced to analyse and evaluate performance. Results declare that the proposed strategy is effective and has the advantages of low time delay, high accuracy and good stability.



check for updates

**Citation:** Chen, J.; Sun, J.; Hu, S.; Ye, Y.; Huang, H.; Tang, C. An effective joint soft-sensing strategy for multi-information under diverse vehicle driving scenarios. *Electronics* **2021**, *10*, 505. <https://doi.org/10.3390/electronics10040505>

Communicated by Andrzej Czyżewski

Received: 13 January 2021

Accepted: 13 February 2021

Published: 21 February 2021

**Publisher's Note:** MDPI stays neutral with regard to jurisdictional claims in published maps and institutional affiliations.



**Copyright:** © 2021 by the authors. Licensee MDPI, Basel, Switzerland. This article is an open access article distributed under the terms and conditions of the Creative Commons Attribution (CC BY) license (<https://creativecommons.org/licenses/by/4.0/>).

**Keywords:** joint soft-sensing strategy; multi-information; time delay; variational Bayesian-based adaptive cubature Kalman filter; cubic observer

## 1. Introduction

In automotive field, the full play performance of active safety system depends on the accurate multi-information including road conditions, vehicle parameters and vehicle states [1–4]. Currently, an economical way to obtain these kinds of information is a soft-sensing approach. However, most of the reported approaches can only be applied under a simplex driving scenario, where the road is flat [5] or the vehicle mass is constant [6]. Actually, due to terrain constraints or design need, the assumption of horizontal road cannot be met, and its mass may vary in several hundred kilograms as a vehicle is full or empty. In addition, there are coupling relationships in the acquisition process of road conditions, vehicle coefficients and vehicle states [2,7–9]. It is helpful to improve the soft-sensing accuracy by integrating multiple information. Hence, it is necessary to study effective joint soft-sensing approach for multi-information.

The traditional joint soft-sensing approaches in the automotive field can be categorized into centralized, reinforced and distributed structures. For the centralized structure, a unified model is utilized to get different information synchronously, which is simple and there is less redundancy. In allusion to road conditions and vehicle parameters, such as the time-varying road slope and vehicle mass, a modified RLS algorithm with multiple forgetting-factors was proposed [10]. In addition, an observer-based scheme with sliding-mode term was developed using onboard sensor signals [3]. Although these above two methods have good accuracy, the road slope results reveal the defect of time delay. However, the centralized structure, in exceptional cases, may present poor accuracy performance or even divergence. Addressing this issue, the reinforced structure was adopted by means of an additional part to enhance the stability of soft-sensing results. For instance, the EKF and

RLS were integrated to obtain the road slope and vehicle mass [11], which provided higher accuracy and faster convergence. In another study, the RLS with multiple factors and EKF are, respectively, adopted in two steps of an estimator, which shows great accuracy and robustness in vehicle road test [12]. Similarly, a two-stage estimation strategy was proposed to determine the road slope and mass of heavy-duty vehicle [9]. However, the design is too complicated and difficult to be applied in practice.

As compared with the centralized structure, the reinforced one has better performance on accuracy and convergence. However, the real-time performance of the latter is dissatisfactory due to its complex construction. As an alternative, the distributed structure employs independent modules to obtain different information, which is beneficial to balance the accuracy and calculation burden. For the module design in the distributed structure, recursive algorithms gain widespread attention, such as the KF [2], observer-based method [4], and RLS [13]. In addition, Hong et al. [14] used three UKFs to obtain the inertial parameters and vehicle states, respectively. However, the complication limits its further generalization. For eliminating the influence of vehicle parameters on vehicle states, Wenzel et al. [8] utilized a DEKF technique, which was primarily proposed by Wan and Nelson [15]. However, this solution does not perform well under ramp road conditions. Moreover, adaptive high-order sliding-mode observer and strong tracking filter were adopted to estimate the information of force, speed and angle for electric vehicle [16]. However, the influence of time-variant noise was not fully considered in its results. Viehweger et al. [17] analyzed four estimation methods about vehicle state and tire force, which shows that the performance of the suboptimal-second order sliding mode and EKF-based method is better in the slow track condition, and the error of the purely linear and EKF-based method is lower in the fast track condition. Considering the complexity of the vehicle's COG in three-dimensional space, a distributed structure-based approach synthesized both vehicle longitudinal and lateral motion, which effectively improves its behaviour [18].

There are also some deficiencies in the traditional joint soft-sensing approaches, such as the time delay of some information and the compatibility for time-variant noise. To lower the time delay, a short-time linear quadratic technique was proposed for the achievement of road slope [19]. However, it is not a good choice because of its complexity. As the consideration of time-variant noise, Berntorp et al. [7,20] adopted a PF framework. However, the calculation of vast particles results in poor real-time performance.

In addition, the response results of the soft-sensing are affected by many factors related to the driver, roadway geometry, environment, vehicle, and so on. It is difficult to consider the interference of all factors in scientific research, or it may lead to a problem called "observational heterogeneity" (the unobservable or unavailable factors in the effect of results that are unknown) [21,22]. If this problem is ignored, the erroneous inferences and predictions that may occur due to the model are misspecified and the estimated parameters are biased [23,24]. Some methods are proposed to deal with it, such as the random parameters method, finite mixtures (latent classes) method and their combination [25,26]. Recently, artificial neural networks have also been used to solve the observational heterogeneity [27].

In case the road conditions change and the vehicle parameters are unknown, it is an important requirement for the automobile development to ensure the effectiveness of soft-sensing. On this basis, an urgent need is to continuously improve the performance of measurement results in terms of accuracy, robustness, time delay, and so on. The motivation of this study is to acquire the vehicle required information even under diverse vehicle driving scenarios. In this paper, a joint soft-sensing strategy is developed to obtain accurate multi-information based on the distributed structure. The information interaction in this strategy is realized according to the coupling relationship among the vehicle state, road slope and vehicle mass. The time-variant noise problem in the vehicle states estimation is adaptively disposed by a VBACKF. To alleviate the time delay of road slope, a slope prediction model is derived to replace the classical road slope model and the corresponding

observer is designed with a cubic term. Finally, the contrast experiment is implemented to evaluate the performance of the proposed strategy.

The rest of this paper is organized as follows. The overview of the strategy is presented in Section 2. The vehicle dynamics model involving road slope is introduced in Section 3. Sections 4–6 show the details on how to achieve the vehicle states, road slope and vehicle mass in turn. The experiment is described in Section 7, and followed by the conclusions in Section 8.

## 2. Joint Soft-Sensing Strategy

Aiming at the problem that the application scenario of most soft-sensing approaches is simple, a joint soft-sensing strategy is proposed. As shown in Figure 1, this strategy mainly consists of three modules: vehicle state estimation, road slope observation and vehicle mass determination. To realize the application of the non-horizontal road scenario, firstly, a vehicle model considering road slope is established. Based on this model, a VBACKF is utilized in the vehicle state estimation module to deal with the time-variant noise via two steps: time update and variational measurement update. In the road slope observation module, a novel slope prediction model and a cubic observer are used to design an observer, which is expected to reduce the time delay. According to the variation character of vehicle mass, a FFRLS algorithm is employed to determine vehicle mass. In addition, the data preprocessing and the threshold judgment steps are added to eliminate the unreliable input data.

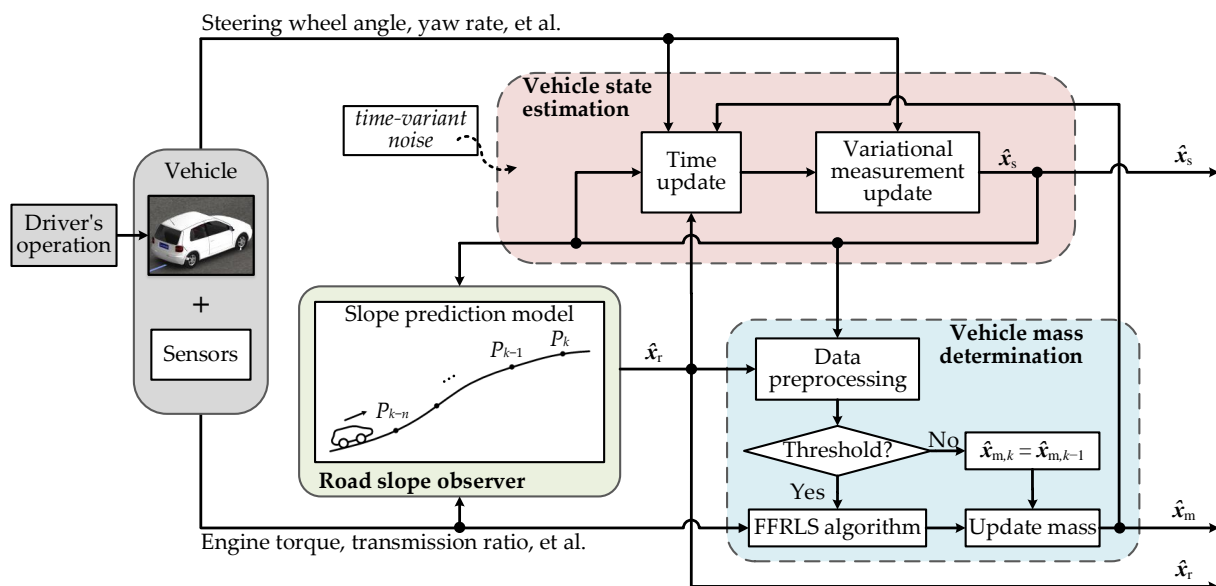


**Figure 1.** The architecture of the joint soft-sensing strategy.

Through this joint soft-sensing strategy, the vehicle state  $\hat{x}_s$ , road slope  $\hat{x}_r$  and vehicle mass  $\hat{x}_m$  are finally obtained, as shown in Figure 1. (Throughout this paper, the superscript “^” means the obtained signals from the strategy.) These data can be used not only to serve as the output, but also to apply to implement the information interaction within the strategy. The vehicle state  $\hat{x}_s$  is adaptively estimated based on the observed road slope from the second module, the determined vehicle mass from the third module and the signals acquired from onboard sensors, such as the steering wheel angle, wheel rotational velocity, vehicle acceleration, and yaw rate. With the estimated value  $\hat{x}_s$ , some onboard sensor signals are also provided for the observation of the road slope, such as the acceleration and yaw rate. Ultimately, by means of the real-time information including the estimated vehicle state  $\hat{x}_s$  and observed road slope  $\hat{x}_r$ , the vehicle mass  $\hat{x}_m$  is determined according to the information from the vehicle system, i.e., the engine torque, transmission ratio, and

braking torque. For this strategy, only the driver’s operation is treated as system input, and there is not any other special sensor equipped.

### 3. Vehicle Dynamics Modelling

Considering that a vehicle’s dynamics characteristic is closely related to road conditions, a nonlinear vehicle model is presented with road slope  $\theta$  (see Figure 2), where COG is the center of gravity, the relationship between the steering wheel angle  $\delta_0$  and the steering angle of front wheels  $\delta$  is assumed as  $\delta_0 = \delta i_w$ ,  $i_w$  is the steering gear ratio of the steering system. The vehicle’s longitudinal, lateral and yaw vehicle motions can be described as

$$\begin{cases} \dot{v}_x = a_x + rv_y \\ \dot{v}_y = a_y - rv_x \\ \dot{r} = M_z/I_z \end{cases}, \quad (1)$$

where  $v_x$  is the longitudinal velocity,  $v_y$  is the lateral velocity,  $r$  is the yaw rate,  $I_z$  is the moment of the inertia around the z-axis,  $a_x$  is the longitudinal acceleration,  $a_y$  is the lateral acceleration,  $M_z$  is the yaw moment.

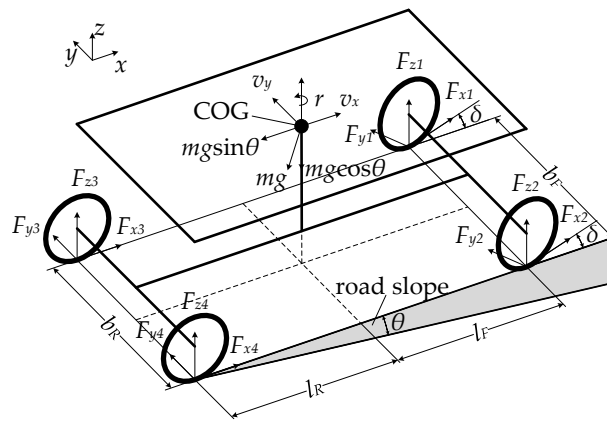


Figure 2. Vehicle model with road slope.

Due to the influence of road slope, the vehicle’s gravity is decomposed into two components:  $mg \sin \theta$  along the x-axis and  $mg \cos \theta$  along the z-axis. The first component mainly affects the vehicle’s longitudinal force

$$a_x = \frac{1}{m} [(F_{x1} + F_{x2}) \cos \delta + F_{x3} + F_{x4} - (F_{y1} + F_{y2}) \sin \delta - \frac{1}{2} C_d A \rho_{\text{air}} v_x^2] - g \sin \theta, \quad (2)$$

where  $m$  is the vehicle mass,  $g$  is the gravitational acceleration,  $F_x$  and  $F_y$  are the longitudinal and lateral tire forces of each wheel, the subscripts 1, 2, 3, 4 represent the left front, right front, left rear and right rear tire,  $C_d$  is the aerodynamic drag coefficient,  $A$  is the frontal area of the vehicle,  $\rho_{\text{air}}$  is the air density.

In addition,  $a_y$ ,  $M_z$  can be expressed as

$$a_y = \frac{1}{m} [(F_{x1} + F_{x2}) \sin \delta + F_{y3} + F_{y4} + (F_{y1} + F_{y2}) \cos \delta], \quad (3)$$

$$\begin{aligned} M_z = & l_F (F_{x1} + F_{x2}) \sin \delta - l_R (F_{y3} + F_{y4}) + l_F (F_{y1} + F_{y2}) \cos \delta - \frac{b_F}{2} (F_{x1} - F_{x2}) \cos \delta \\ & + \frac{b_F}{2} (F_{y1} - F_{y2}) \sin \delta - \frac{b_R}{2} (F_{x3} - F_{x4}), \end{aligned} \quad (4)$$

where  $l_F$  and  $l_R$  are the distances from the COG to front and rear axles,  $b_F$  and  $b_R$  are the front and rear track width.

As a result of the component along the z-axis, the vertical tire forces on each tire  $F_z$  are

$$\begin{cases} F_{z1,2} = \frac{ml_R g \cos \theta}{2(l_F + l_R)} - \frac{mha_x}{2(l_F + l_R)} \mp \frac{mhl_R a_y}{(l_F + l_R)b_F} \\ F_{z3,4} = \frac{ml_F g \cos \theta}{2(l_F + l_R)} + \frac{mha_x}{2(l_F + l_R)} \mp \frac{mhl_F a_y}{(l_F + l_R)b_R} \end{cases}, \tag{5}$$

where  $h$  is the height of COG.

The wheel side angle  $\alpha_t$ , wheel slip rate  $\sigma$  and forward wheel speed  $v_t$  are presented as

$$\begin{cases} \alpha_{t1,2} = \delta - \arctan\left(\frac{(v_y + l_F r)}{(v_x \mp \frac{b_F}{2} r)}\right) \\ \alpha_{t3,4} = \arctan\left(\frac{(-v_y + l_R r)}{(v_x \mp \frac{b_R}{2} r)}\right) \end{cases}, \tag{6}$$

$$\begin{cases} v_{t1,2} = \left(v_x \mp \frac{b_F}{2} r\right) \cos \delta + (v_y + l_F r) \sin \delta \\ v_{t3,4} = v_x \mp \frac{b_R}{2} r \end{cases}, \tag{7}$$

$$\sigma = \omega R_t / v_t - 1, \tag{8}$$

where  $\omega$  is the wheel rotational speed,  $R_t$  is the wheel radius.

In this study, we use the Dugoff tire model [28] to generate the longitudinal and lateral tire forces, because of its good behavior in online computation and accuracy. As follows

$$\begin{cases} F_x = \frac{C_\sigma \sigma}{1 + \sigma} f(\lambda) \\ F_y = \frac{C_\alpha \tan \alpha_t}{1 + \sigma} f(\lambda) \end{cases}, \text{ where } \begin{cases} \lambda = \frac{\mu F_z (1 + \sigma)}{2\sqrt{(C_\sigma \sigma)^2 + (C_\alpha \tan \alpha_t)^2}} \\ f(\lambda) = \begin{cases} 1, & \lambda \geq 1 \\ (2 - \lambda)\lambda, & \lambda < 1 \end{cases} \end{cases}, \tag{9}$$

where  $C_\sigma$  and  $C_\alpha$  are the longitudinal and lateral wheel stiffnesses.  $\lambda$  is the model parameter,  $\mu$  is the road adhesion coefficient.

#### 4. Vehicle State Estimation

On the basis of the vehicle model in Figure 2, the continuous state space for vehicle state estimation can be written as follows

$$\begin{cases} \dot{x}_s = f(x_s, u_s) + v \\ z_s = h(x_s) + w \end{cases}, \tag{10}$$

where  $f(\cdot), h(\cdot)$  are the process and measurement functions,  $x_s = [v_x \ v_y \ r \ a_x \ a_y]^T$  is the state vector, the input vector  $u_s = [\delta \ \omega_i \ \hat{\theta} \ \hat{m}]^T$ , the measurement vector  $z_s$  consists of the longitudinal acceleration, lateral acceleration and yaw rate,  $v$  and  $w$  are the process and measurement noises with the covariance matrices  $Q$  and  $R$ .

In the framework of the CKF, the measurement noise is assumed as Gaussian white noise with constant mean and covariance [29]. This signifies that it is indispensable for good soft-sensing results to get the feature of measurement noise covariance [30]. However, time-variant noise covariance is a prevalent problem in practical application. It even has been one of the main reasons that lead to the divergence of estimation result [20,31]. In this study, the VBACKF is employed to handle the issue of time-variant noise.

Firstly, the conjugate prior distributions need to be selected for the measurement noise covariance matrix  $R_k$  at time  $k$  since the conjugacy can guarantee that the posterior distribution is of the same functional form as the prior distribution [30]. In Bayesian statistics, the IW distribution is usually used as the conjugate prior for the covariance

matrix [32], i.e.,  $p(\mathbf{R}_k | z_{s,1:k-1}) \sim IW(\mathbf{R}_k; v_k, \mathbf{V}_k)$ . where  $\mathbf{V}_k$  is the inverse scale matrix representing a symmetric positive definite matrix with the dimension of  $d \times d$ ,  $v_k$  is the degrees of freedom parameter, and the noise covariance matrix  $\mathbf{R}_k$  is represented by the mean of the IW distribution

$$E(\mathbf{R}_k) = \mathbf{V}_k / (v_k - d - 1). \tag{11}$$

Based on the mean field theory, the joint probability density function  $p(\mathbf{x}_{s,k}, \mathbf{R}_k | z_{s,1:k})$  of the vehicle state  $\mathbf{x}_{s,k}$  and measurement noise  $\mathbf{R}_k$  is expressed as the product of their approximate probability density function  $q(\mathbf{x}_{s,k})$  and  $q(\mathbf{R}_k)$

$$p(\mathbf{x}_{s,k}, \mathbf{R}_k | z_{s,1:k}) \approx q(\mathbf{x}_{s,k})q(\mathbf{R}_k). \tag{12}$$

The approximate solutions of the  $q(\mathbf{x}_{s,k})$  and  $q(\mathbf{R}_k)$  can be obtained by minimizing the KLD

$$\{q(\mathbf{x}_{s,k}), q(\mathbf{R}_k)\} = \arg \min \text{KLD}(q(\mathbf{x}_{s,k})q(\mathbf{R}_k)p(\mathbf{x}_{s,k}, \mathbf{R}_k | z_{s,1:k})). \tag{13}$$

Based on the VBACKF algorithm, the vehicle state estimation module contains two steps: time update and variational measurement update, as shown in Figure 3. The time update realizes the prediction of the vehicle state vector  $\mathbf{x}_s$  and its covariance matrix  $\mathbf{P}$  through the cubature points. Subsequently, the time-variant measurement noise covariance matrix  $\mathbf{R}$  is also predicted out in this part. For another part, the vehicle state vector  $\mathbf{x}_s$  is updated not only through the cubature points, but also by means of the variational iteration. Meanwhile, the time-variant measurement noise covariance matrix  $\mathbf{R}$  is adaptively characterized by use of the variational iteration as well. It should be noticed that the number  $N$  is an important parameter used to balance the accuracy and real-time performance [30].

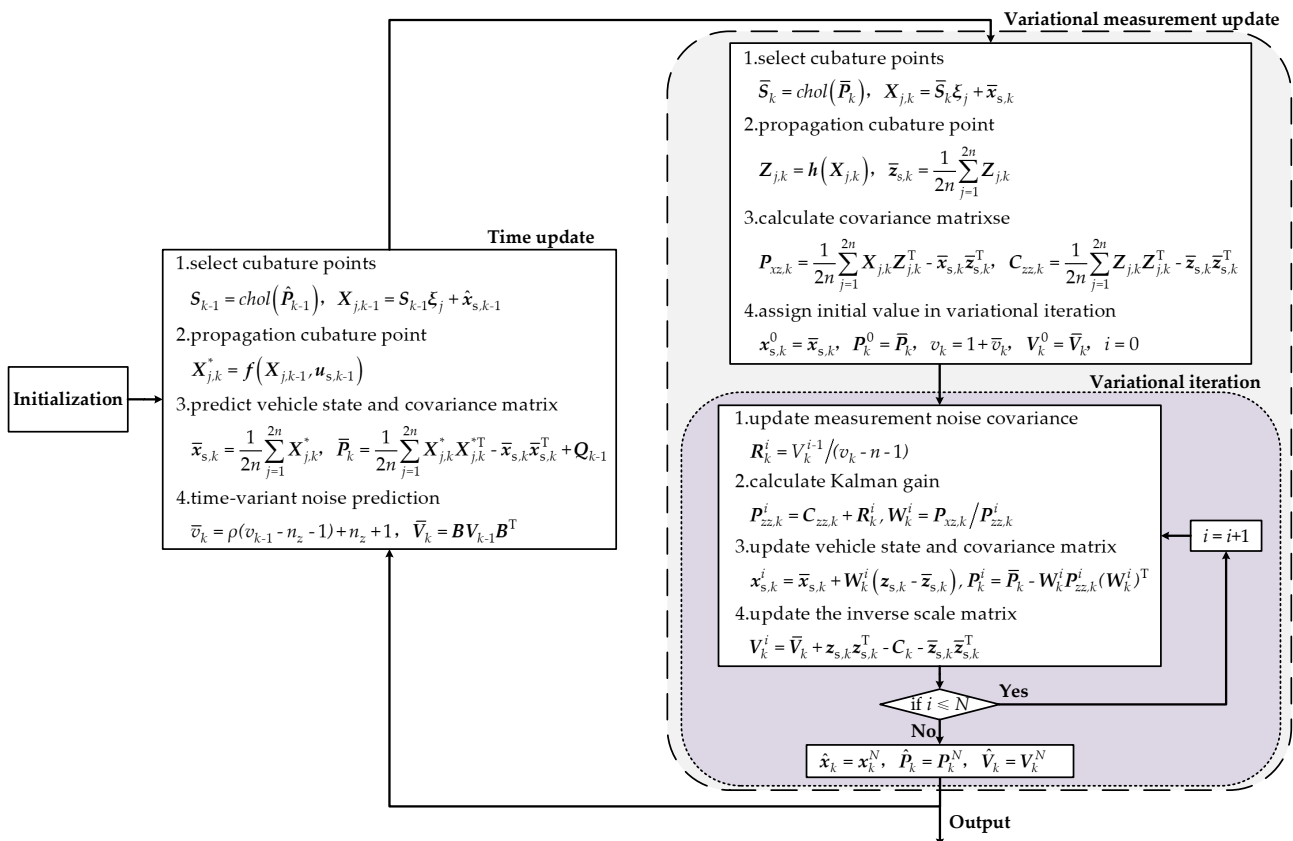


**Figure 3.** Flow chart of vehicle state estimation based on the VBACKF algorithm. Where  $\mathbf{S}$  is the state covariance factor,  $\mathbf{X}$  is the cubature points,  $\boldsymbol{\zeta}$  is the standard cubature points,  $\rho$  is the tuning parameter,  $\mathbf{B}$  is the adjustment matrix,  $\mathbf{Z}$  is the propagated measurement matrix,  $\mathbf{P}_{xz}$  is the cross-covariance matrix,  $\mathbf{C}_{zz}$  is the partial measurement noise covariance,  $\mathbf{P}_{zz}$  is the measurement noise covariance matrix,  $\mathbf{W}$  is the Kalman gain.

Based on the estimation results of vehicle longitudinal velocity  $\hat{v}_x$  and lateral velocity  $\hat{v}_y$ , vehicle sideslip angle  $\beta$  can be calculated as follows

$$\beta = \arctan(\hat{v}_y/\hat{v}_x). \tag{14}$$

### 5. Road Slope Observation

For the classical road slope model  $\dot{\theta} = 0$ , its change rate is assumed to be invariable since the road slope usually changes slowly and weak in short distance [9,11]. However, this change should not be completely neglected; otherwise, a “time delay” problem occurs in the observation curve, particularly for variable terrain [33,34]. To alleviate the time delay, a slope prediction model is derived for the observation of real-time road slope.

#### 5.1. Slope Prediction Model

Due to practical requirements, road needs to keep continuous and its slope can not change suddenly. Under this consideration of road continuity, a slope prediction model is presented for the observation of road slope. Figure 4 shows the cases that a vehicle goes up or down a hill, where  $P_k, P_{k-1}, \dots, P_{k-n+1}$  and  $P_{k-n}$  mean vehicle location at different time points. Assuming that the road slope  $\theta_{k-n}$  and vehicle longitudinal velocity  $v_{x,k-n}$  at points  $P_{k-n}$  ( $1 \leq n < k$ ) are all known. The road slope  $\theta_k$  at current location  $P_k$  can be acquired via an observer.

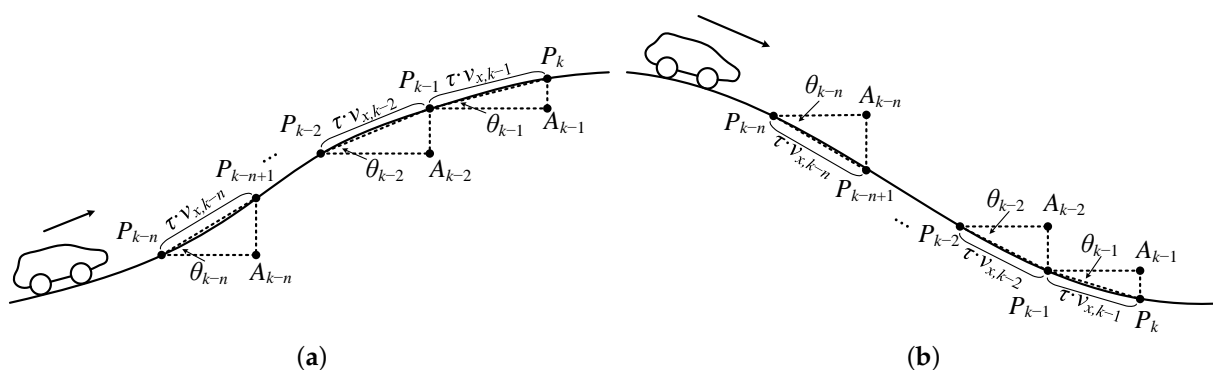


Figure 4. Slope prediction model. (a) Case:  $\theta > 0$ . (b) Case:  $\theta < 0$ .

The distance between two adjacent points  $|P_{k-n}P_{k-n+1}|$  can be approximately denoted as

$$|P_{k-n}P_{k-n+1}| = \tau v_{x,k-n}, \tag{15}$$

where  $\tau$  is the sampling time. The relationships among the edges of the dashed line triangles in Figure 4 can be expressed as

$$\begin{aligned} |A_{k-n}P_{k-n}| &= |P_{k-n}P_{k-n+1}| \cos \theta_{k-n} \\ |A_{k-n}P_{k-n+1}| &= |P_{k-n}P_{k-n+1}| \sin \theta_{k-n} \end{aligned} \tag{16}$$

If we establish a two-dimensional coordinate frame  $x$ - $o$ - $y$  at point  $P_{k-1}$  (the  $x$ -axis direction is along  $P_{k-1}A_{k-1}$ , and the  $y$ -axis direction is along  $A_{k-2}P_{k-1}$ ), the coordinates for every point are as follows

$$\begin{cases} P_k : (|A_{k-1}P_{k-1}|, |A_{k-1}P_k|) \rightarrow (\tau v_{x,k-1} \cos \theta_{k-1}, \tau v_{x,k-1} \sin \theta_{k-1}) \\ P_{k-1} : (0, 0) \\ P_{k-n} : \left( -\sum_{j=2}^n |A_{k-j}P_{k-j}|, -\sum_{j=2}^n |A_{k-j}P_{k-j+1}| \right) \end{cases} \tag{17}$$

To describe the partial road trait at the coordinate point  $(x, y)$ , the following second-order form is utilized

$$y = a_1x + a_2x^2, \quad (18)$$

where  $a_1$  and  $a_2$  are the fitting parameters. Furthermore, as the consideration that practical road slope  $\theta$  is relatively small ( $\theta \leq 0.08$  rad  $\approx 15$  deg), the relationship between the road slope and the corresponding point can be determined by derivating Equation (18), i.e.,

$$\theta \approx \tan \theta = \dot{y} = a_1 + 2a_2x. \quad (19)$$

Hence, the parameters  $a_1$  and  $a_2$  can be fitted by Equation (19) instead of the second-order form with the information at points  $P_{k-n}$  ( $1 \leq n < k$ ). As shown in the following equation, the slope prediction model reflecting the change rate of road slope is derived from the second derivative of Equation (18).

$$\dot{\theta} = \dot{y} = 2a_2. \quad (20)$$

Different from the classical road slope model  $\dot{\theta} = 0$ , the slope prediction model is expected to improve the accuracy by gaining the change rate of the current road slope.

### 5.2. Observer Design for Road Slope

In the design processing of the traditional Luenberger observer, its error dynamics emerge as linear characteristics [35]. Limited by this reason, the response rate of this kind of observer does not perform well. However, research shows that an observer with fast response may alleviate the time delay to some extent [36]. In this section, a cubic observer with nonlinear error dynamics is introduced to observe road slope. Compared to the Luenberger observer, the cubic observer contains a cubic error dynamics term and has a faster descending Lyapunov function when error norms are equal [37].

For a vehicle driving on a ramp, the output of the equipped longitudinal accelerometer  $a_{x,acc}$  can be remarked as  $a_{x,acc} = \dot{v}_x - rv_y + g \sin \theta$  [2,13]. Considering the relatively small road slope, it can be expressed as

$$a_{x,acc} \approx \dot{v}_x - rv_y + g\theta. \quad (21)$$

Combining this formula with Equation (20), we can obtain the following state space

$$\begin{cases} \dot{\mathbf{x}}_r = \mathbf{A}\mathbf{x}_r + \mathbf{\Phi}\mathbf{u}_r \\ \mathbf{y}_r = \mathbf{C}\mathbf{x}_r \end{cases}, \quad (22)$$

where the state vector  $\mathbf{x}_r = [v_x \ \theta]^T$ , the measurement vector  $\mathbf{y}_r = [v_x]^T$ , the input vector  $\mathbf{u}_r = [u_1 \ 2a_2]^T$  (here  $u_1$  is set as  $u_1 = a_{x,acc} + r\dot{v}_y$ ), and the matrixes  $\mathbf{A}$ ,  $\mathbf{\Phi}$  and  $\mathbf{C}$  are as follows

$$\mathbf{A} = \begin{bmatrix} 0 & -g \\ 0 & 0 \end{bmatrix}, \mathbf{\Phi} = \begin{bmatrix} 1 & 0 \\ 0 & 1 \end{bmatrix}, \mathbf{C} = [1 \ 0]. \quad (23)$$

To complete the observation of road slope, the cubic observer is employed based on the state space

$$\dot{\hat{\mathbf{x}}}_r = (\mathbf{A} - \mathbf{L}_c\mathbf{C})\hat{\mathbf{x}}_r + \mathbf{L}_c\mathbf{y}_r + \mathbf{\Phi}\mathbf{u}_r - \mathbf{e}_c^T\mathbf{C}^T\boldsymbol{\kappa}_c\mathbf{C}\mathbf{e}_c\mathbf{N}_c\mathbf{C}\mathbf{e}_c, \quad (24)$$

where  $\hat{\mathbf{x}}_r$  is the reconstructed state,  $\mathbf{L}_c$ ,  $\boldsymbol{\kappa}_c$  and  $\mathbf{N}_c$  are the observer parameter matrices and estimation error  $\mathbf{e}_c = \mathbf{x}_r - \hat{\mathbf{x}}_r$ .

The observer is globally stable when the following error dynamic  $\dot{\mathbf{e}}_c$  converges

$$\dot{\mathbf{e}}_c = (\mathbf{A} - \mathbf{L}_c\mathbf{C})\mathbf{e}_c + \mathbf{e}_c^T\mathbf{C}^T\boldsymbol{\kappa}_c\mathbf{C}\mathbf{e}_c\mathbf{N}_c\mathbf{C}\mathbf{e}_c. \quad (25)$$

Equation (25) is equal to zero only when the condition  $e_c = 0$  is met. Defining the Lyapunov function candidate  $V_c = e_c^T P_c e_c$ , where  $P_c = P_c^T \geq 0$ . The stability criterion can be written as

$$e_c^T \left( (A - L_c C)^T P_c + P_c (A - L_c C) \right) e_c + \left( e_c^T C^T \kappa_c C e_c \right) \times e_c^T \left( P_c N_c C + C^T N_c^T P_c \right) e_c < 0. \tag{26}$$

It can be transformed into the following form

$$\begin{cases} (A - L_c C)^T P_c + P_c (A - L_c C) < 0 \\ P_c N_c C + C^T N_c^T P_c < 0 \end{cases}. \tag{27}$$

By derivation, Equation (27) works if the following conditions are satisfied, i.e., the matrices  $\kappa_c = \kappa_c^T \geq 0$ ,  $N_c = -\gamma P_c^{-1} C^T \kappa_c$  (scalar  $\gamma > 0$  is arbitrary) and  $L_c$  need to be tuned.

### 6. Vehicle Mass Determination

Current methods for obtaining vehicle mass are usually based on longitudinal vehicle dynamics [9,10], where only the driving torque is involved. To further reflect practical condition for application, it is replaced by the following equation with the braking effect:

$$\frac{T_{tq} i_g i_0 \eta_t}{R_t} = mg \sin \theta + mg \zeta \cos \theta + m \dot{v}_x + \frac{1}{2} C_d A \rho_{air} v_x^2 + \frac{T_b}{R_t}, \tag{28}$$

where  $T_{tq}$  is the engine output torque,  $i_g$  is the transmission ratio,  $i_0$  is the main reducer transmission ratio,  $\eta_t$  is the mechanical efficiency of the drive train,  $T_b$  is the braking torque, and  $\zeta$  is the rolling resistance coefficient.

The equation can be linearized under the conditions that  $\sin \theta \approx \theta$  and  $\cos \theta \approx 1$ , i.e.,

$$\Omega_m \hat{x}_m = y, \tag{29}$$

where the unknown parameter  $\hat{x}_m = m$ , the observed data  $y = (T_{tq} i_g i_0 \eta_t - T_b) / R_t - C_d A \rho_{air} v_x^2 / 2$  and  $\Omega_m = g \hat{\theta} + g \zeta + \dot{v}_x$  (here  $\hat{\theta}$  and  $\dot{v}_x$  are the signals from other modules).

Based on Equation (29), the FFRLS algorithm [10,11] is employed to determine the vehicle mass.

To determine the vehicle mass, the FFRLS algorithm [10,11] is employed based on Equation (29), where the forgetting-factor  $\lambda_m$  should be tuned.

$$\begin{cases} K_{m,k} = P_{m,k-1} \Omega_{m,k} / \left( \lambda_m + \Omega_{m,k}^T P_{m,k-1} \Omega_{m,k} \right) \\ \hat{x}_{m,k} = \hat{x}_{m,k-1} + K_{m,k} \left( y_k - \Omega_{m,k}^T \hat{x}_{m,k-1} \right) \\ P_{m,k} = \left( P_{m,k-1} - K_{m,k} \Omega_{m,k}^T P_{m,k-1} \right) / \lambda_m \end{cases}, \tag{30}$$

where  $K_m$  is the least squares gain,  $P_m$  is the covariance.

As mentioned above, the vehicle mass determination module will accept the vehicle state and road slope data. To improve the reliability of the data, the data preprocessing and the threshold judgment steps are added. The corresponding expression is as follows:

$$\begin{aligned} \varepsilon &= |g \hat{\theta} + g f + \dot{v}_x| \\ \varepsilon &\geq \text{threshold} \end{aligned}, \tag{31}$$

where  $\varepsilon$  is the result of the data preprocessing. Once the threshold condition is satisfied, the vehicle mass is determined by the FFRLS algorithm. Otherwise, it remains the same as the last moment.

### 7. Verification for Joint Strategy

Based on the computer and driving simulator, the experiments under diverse driving scenarios are implemented to verify the effectiveness of the joint soft-sensing strategy. To

facilitate performance comparison, a contrasted strategy is introduced, where the CKF and classical road slope model are utilized to replace the VBACKF and slope prediction model in the proposed strategy. As for the road slope observation, the classical road slope model  $\dot{\theta} = 0$  is combined with Equation (21) to form the state space as

$$\begin{cases} \dot{x}_{r,con} = A_{con}x_{r,con} + \Phi_{con}u_{r,con} \\ y_{r,con} = C_{con}x_{r,con} \end{cases} \quad (32)$$

where the state vector  $x_{r,con} = [v_x \ \theta]^T$ , the measurement vector  $y_{r,con} = [v_x]^T$ , the input vector  $u_{r,con} = [u_1 \ 0]^T$ , and the matrixes  $A_{con}$ ,  $\Phi_{con}$  and  $C_{con}$  are as follows

$$A_{con} = \begin{bmatrix} 0 & -g \\ 0 & 0 \end{bmatrix}, \Phi_{con} = \begin{bmatrix} 1 & 0 \\ 0 & 0 \end{bmatrix}, C_{con} = [1 \ 0]. \quad (33)$$

Based on this state space, the cubic observer in the contrasted strategy can be designed.

### 7.1. Simulation

The construction for simulation is based on the MATLAB/Simulink and CarSim (see Figure 5), where a D-Class Sedan is selected as the experimental vehicle. The relevant vehicle parameters are listed in Table 1, and the initial values of vehicle mass and longitudinal velocity are set as 1300 kg and 80 km/h.

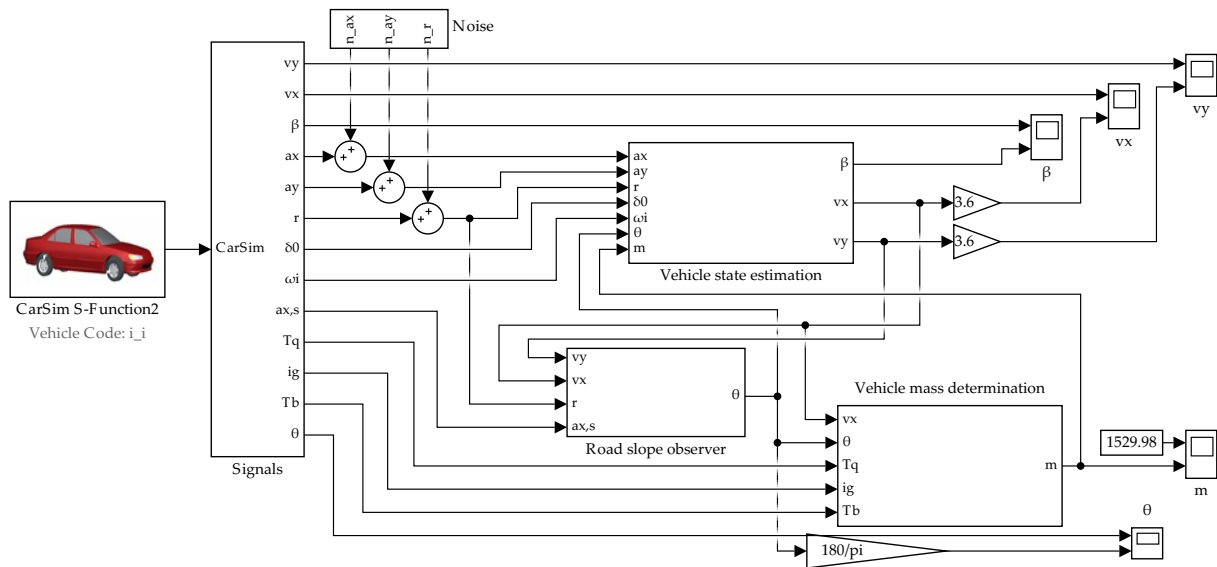


Figure 5. Construction for simulation.

Table 1. Vehicle parameters.

Parameter	Value	Parameter	Value
$m$ (kg)	1529.98	$i_w$	19
$l_F$ (m)	1.139	$\zeta$	0.013
$l_R$ (m)	1.637	$\eta_t$	0.89
$b_F$ (m)	1.550	$i_0$	4.1
$b_R$ (m)	1.550	$A$ (m <sup>2</sup> )	2.4
$I_z$ (kg · m <sup>2</sup> )	4607.47	$C_d$	0.3
$g$ (m/s <sup>2</sup> )	9.8	$\rho_{air}$ (kg/m <sup>3</sup> )	1.206
$h$ (m)	0.519	$R_f$ (m)	0.325

In the vehicle state estimation module, the initial value  $x_{s0}$  and covariance matrix  $P_0$  for state vector are  $x_{s0} = [80/3.6 \ 0 \ 0 \ 0 \ 0]^T$  and  $P_0 = I_{5 \times 5} \times 10$ , the process

noise covariance matrix  $Q = I_{5 \times 5} \times 0.1$ , and the measurement noise covariance matrix  $R = \text{diag}[4 \times 10^{-2} \ 4 \times 10^{-2} \ 6 \times 10^{-5}]$ . In addition, the sampling time  $\tau$  is 0.01 s, the matrix in the cubic observer is chosen as  $L_c = [1 \ -2]^T$ , and the forgetting-factor for the FFRLS algorithm is 0.998.

The top view of the experimental trajectory is shown in Figure 6a, which is a 2328-m-long enclosed road starting from point O and along the arrow direction, the relationship between the road elevation and driving route is revealed in Figure 6b, and the corresponding signals of the steering wheel angle  $\delta_o$  and wheel rotational speed  $\omega$  are plotted in Figure 7. For the enclosed trajectory representing the diverse vehicle driving scenarios, the cycle driving time is about 150 s. On this basis, we use the following matrix to simulate the time-variant measurement noise environment:

$$R_{\text{set}} = \begin{cases} 9R & t \leq 40 \\ R & 40 < t \leq 80 \\ 4R & 80 < t \leq 120 \\ 0.25R & 120 < t \leq 160 \end{cases} \quad (34)$$

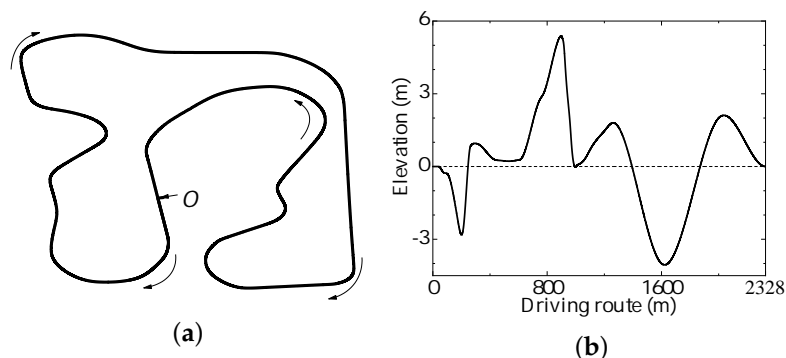


Figure 6. Experimental trajectory. (a) Top view. (b) Elevation vs. driving route.

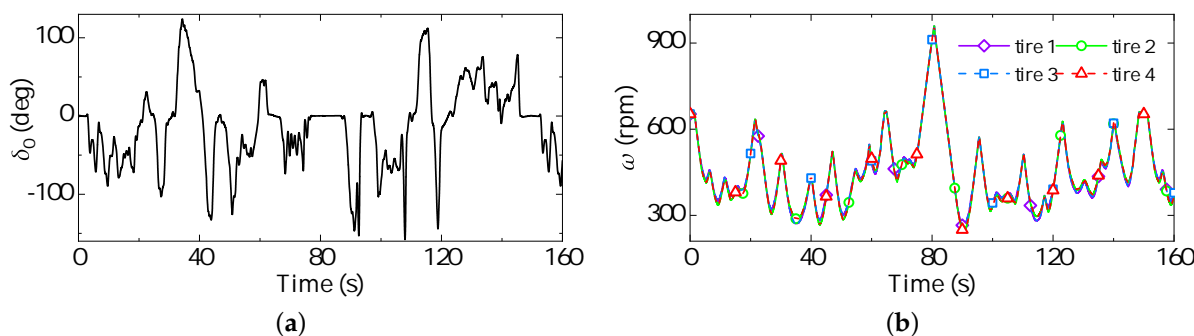
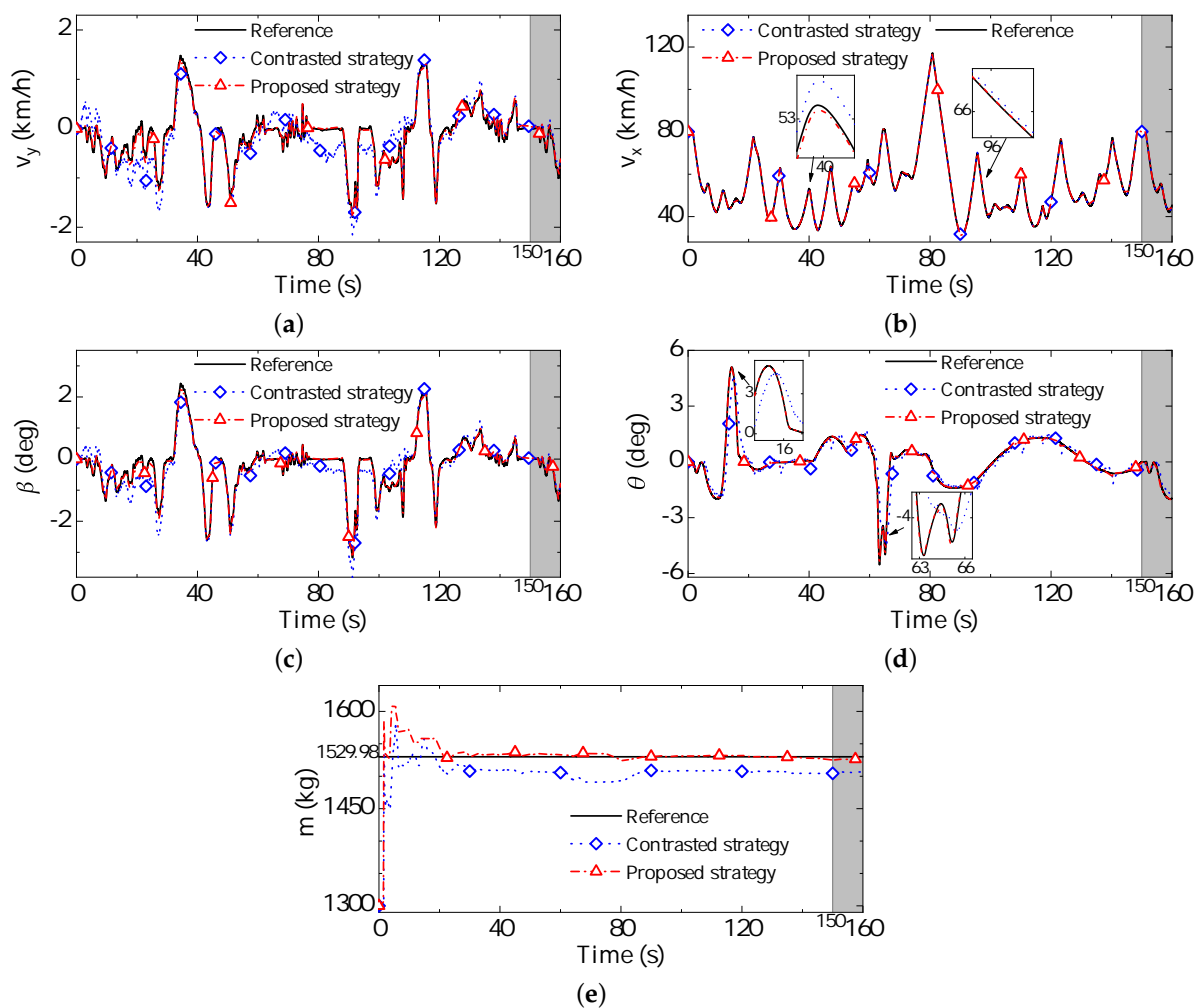


Figure 7. System input signals. (a) Steering wheel angle. (b) Wheel rotational speed.

The experimental results of multi-information are shown in Figure 8, where the shadow part represents the new cycle. It can be found that in the enlarged parts of Figure 8b, the result of the longitudinal velocity is closer to the reference when the proposed strategy is employed. Similar tendencies apparently exist in the interval [60 s, 10 s] of Figure 8a and the interval [80 s, 110 s] of Figure 8c. Especially for the observation result of the road slope in Figure 8d, there is a conspicuous time lag deriving from the contrasted strategy. That is the so-called time delay. Meanwhile, for the proposed strategy, the phenomenon of time delay is so inapparent that it can not be displayed as compared with the contrasted one. The determined vehicle mass of the proposed strategy in Figure 8e is closer to the reference as well.



**Figure 8.** Experimental results of multi-information. (a) Lateral velocity. (b) Longitudinal velocity. (c) Sideslip angle. (d) Road slope. (e) Vehicle mass.

In order to evaluate the accuracy performance, the error curves of these two strategies are given in Figure 9, where the prefix e stands for error. The curves in Figure 9a declare that the error of the lateral velocity provided by the proposed strategy is smaller as a whole. This should be owed to the inherent trait of the VBACKF over time-variant measurement noise, i.e., noise robustness. By comparison and analysis, we confirm that there are analogous consequences of the error curves in the other parts of Figure 9.

Meanwhile, we present the corresponding statistical indicators of the experimental results, such as the MAE and RMSE (see Figure 10). It can be seen from Figure 10a that the MAEs of the lateral velocity, longitudinal velocity, sideslip angle, road slope and vehicle mass are lowered by 80.006%, 71.425%, 79.651%, 89.863% and 69.235%, respectively, when the proposed strategy is employed. The same dominance from the proposed strategy is revealed by the statistical results in Figure 10b involving the RMSE.

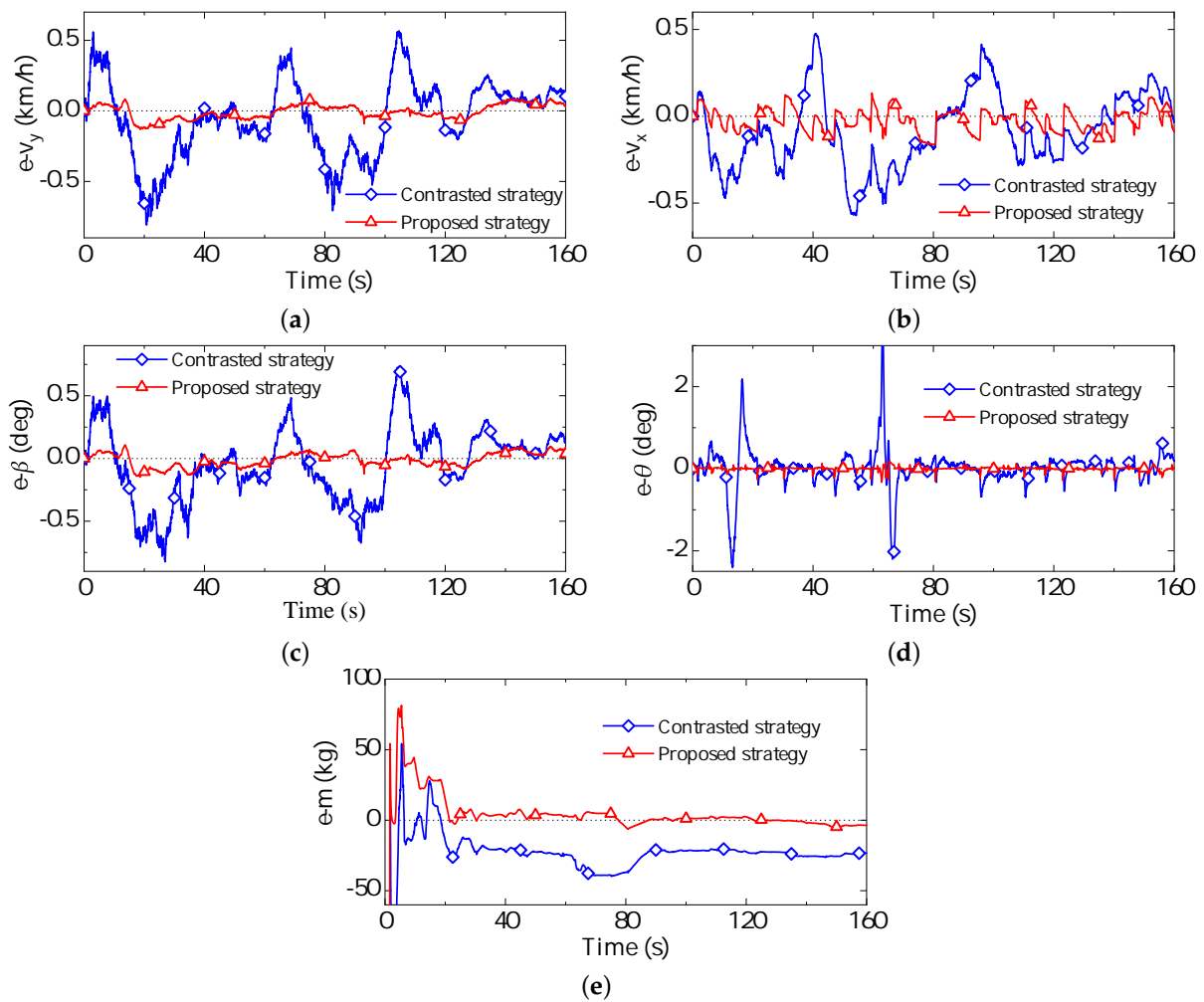


**Figure 9.** Error curves of experimental results. (a) Lateral velocity. (b) Longitudinal velocity. (c) Sideslip angle. (d) Road slope. (e) Vehicle mass.

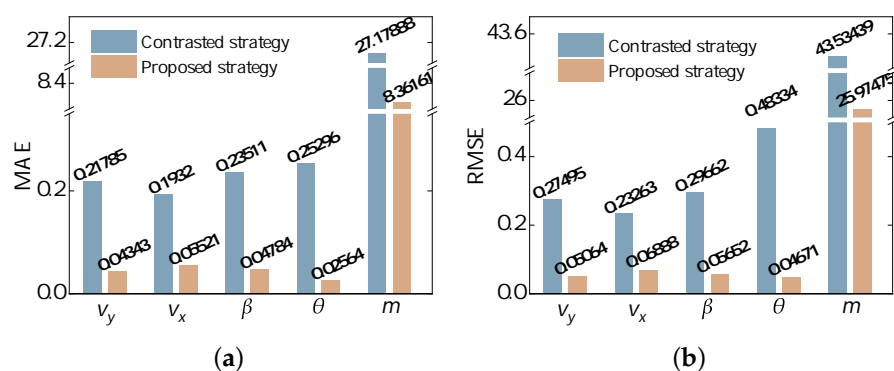


**Figure 10.** Statistical results of simulation. (a) MAE. (b) RMSE.

To further illustrate the performance superiority of the proposed strategy, the frequency distribution histograms of experimental errors are drawn in Figure 11. It is obvious that the error distribution of the proposed strategy is concentrated around zero while that of the contrasted one is relatively dispersed. This suggests that utilizing the proposed strategy, we can obtain experimental results with better error distribution even under diverse vehicle driving scenarios. To some extent, it can be attributed as a kind of good stability for the soft-sensing result.

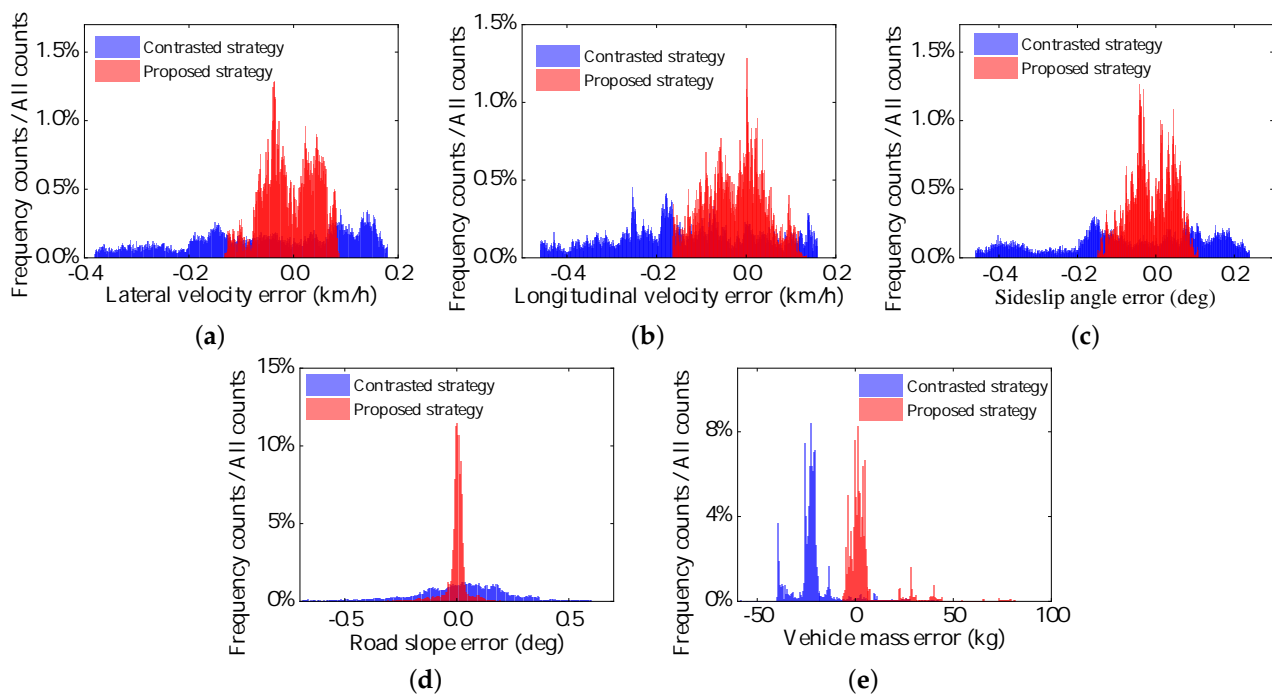


**Figure 11.** Frequency distribution histograms of experimental errors. (a) Lateral velocity. (b) Longitudinal velocity. (c) Sideslip angle. (d) Road slope. (e) Vehicle mass.

On the basis of the result analysis mentioned above, it can be confirmed that the proposed strategy can effectively accomplish the joint soft-sensing of multi-information including the vehicle state, road slope, and vehicle mass. In brief, the advantage of this strategy focuses on the performance of low time delay, high accuracy and good stability.

For the improvement of time delay, it can be attributed to the utilization of the slope prediction model and the nonlinear cubic observer in the module of road slope observation. By means of which, under the assumption of road continuity, even rapidly changed road slope can be iteratively predicted (see the interval (10 s, 20 s) and (60 s, 70 s) of Figure 9d). Moreover, the good performance of accuracy and stability is mainly related to the VBACKF employed in the module of vehicle state estimation. Based on the variational iteration in the VBACKF, the time-variant measurement noise is adaptively characterized and treated as a necessary part for variational measurement update. Of course, the information interaction itself tends to the improvement of accuracy and stability performance because the proposed strategy is good at iteratively making use of inner information. That is also the main reason why vehicle mass accuracy is improved.

## 7.2. Driving Simulator Experiment

The driving simulator used in this experiment is provided by FORUM8, as Figure 12. The driver is a 27-year-old male with three years of driving experience. The initial vehicle speed is 76 km/h, the vehicle mass is 2850 kg and the input signal of steering wheel is shown in Figure 13.

The results of vehicle states in Figure 14a–c show that the proposed strategy can follow the reference better in the most process, while there is a large deviation in the contrasted strategy. In the interval (9 s, 11 s) in Figure 14d, the time delay of the proposed strategy is significantly smaller than the other. As for the vehicle mass in Figure 14e, the proposed strategy reveals smaller errors as well.

The MAE and RMSE indicators of the driving simulator experiment are presented in Figure 15. It is easy to see that the indicators of the proposed strategy are lower than the contrasted one. This proves that the proposed strategy's performance is improved in statistical sense.



Figure 12. Driving simulator operation demonstration.

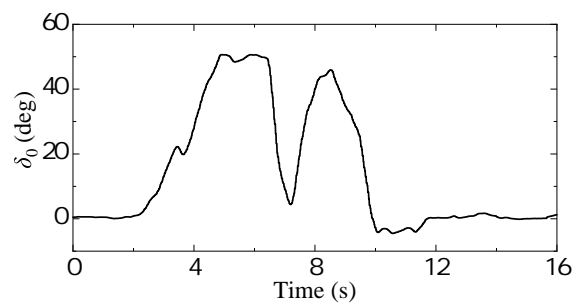


Figure 13. Driver input signals of steering wheel angle.

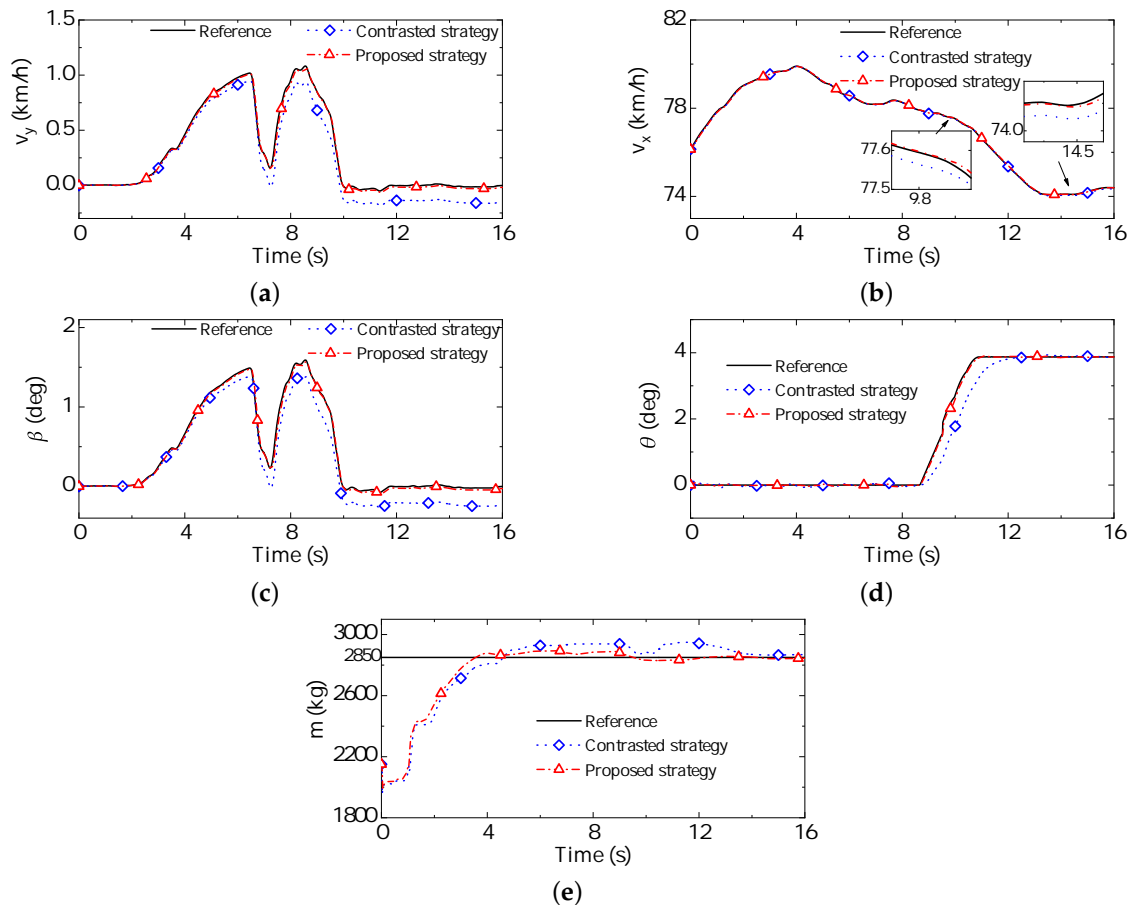


Figure 14. Experimental results of multi-information (driving simulator). (a) Lateral velocity. (b) Longitudinal velocity. (c) Sideslip angle. (d) Road slope. (e) Vehicle mass.

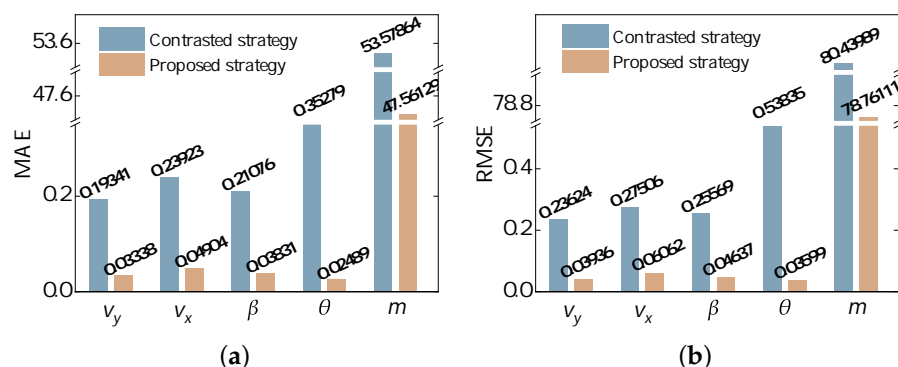


Figure 15. Statistical results of driving simulator experiment. (a) MAE. (b) RMSE.

In general, the above-mentioned results demonstrate the effectiveness of the proposed joint soft-sensing strategy under diverse vehicle driving scenarios. Three modules in the strategy respectively implement the functions of estimating the vehicle state robustly, reducing the time delay of road slope observation and tracking the mutated vehicle mass. What is more, the information interaction within the strategy also provides virtual support for high-performance acquisition of multi-information.

## 8. Conclusions

This paper presents a joint soft-sensing strategy that can provide multi-information for automotive control under diverse vehicle driving scenarios. According to the distributed structure, the joint strategy realizes an information interaction among three modules. Based on the vehicle dynamic considering the road slope, the VBACKF is employed to adaptively estimate the vehicle states. To reduce the time delay, the road slope observer is implemented utilizing the slope prediction model and a fast response nonlinear cubic observer. The accuracy of vehicle mass is guaranteed by the information interaction and threshold judgment. Experimental results under diverse vehicle driving scenarios indicate the effectiveness of the proposed strategy and its performance superiority of low time delay, high accuracy and good stability.

For the development of the automated vehicle technology, this study may provide a new line of thinking for information soft-sensing and provide a necessary information guarantee for vehicle decision-planning and control.

Noticing that the omission of some potential factors may lead to unobserved heterogeneity, further research will be done on the accurate vehicle dynamics model, the position change of the COG, road adhesion coefficient, and so on. The real vehicle experiments will be carried out to make up for the unknown shortcoming in data.

**Author Contributions:** Conceptualization, J.C. and J.S.; methodology, J.C. and J.S.; software, S.H.; validation, J.C., J.S. and C.T.; formal analysis, C.T.; investigation, Y.Y.; resources, H.H.; data curation, S.H.; writing—original draft preparation, J.S.; writing—review and editing, J.C.; visualization, Y.Y.; supervision, J.C. and C.T.; project administration, J.C.; funding acquisition, J.C. All authors have read and agreed to the published version of the manuscript.

**Funding:** This work was supported in part by the National Natural Science Foundation of China (grant # 52072159, 61603158 and 51405203), the China Postdoctoral Science Foundation (grant # 2017M611711 and 2016M601727), the Six Talent Peaks Project in Jiangsu Province (grant # 2016-JXQC-007).

**Institutional Review Board Statement:** Not applicable.

**Informed Consent Statement:** Not applicable.

**Data Availability Statement:** Limited data available on request due to the 3rd party data.

**Conflicts of Interest:** The authors declare no conflict of interest.

## Abbreviations

The following abbreviations are used in this manuscript:

RLS	recursive least square
EKF	extended Kalman filter
KF	Kalman filter
COG	center of gravity
UKF	unscented Kalman filter
DEKF	dual extended Kalman filter
PF	particle filter
VBACKF	variational Bayesian-based adaptive cubature Kalman filter
FFRLS	forgetting-factor RLS
CKF	cubature Kalman filter
IW	inverse Wishart
KLD	Kullback-Leibler divergence
MAE	mean absolute error
RMSE	root mean square error

## References

- Guo, H.; Yin, Z.; Cao, D.; Chen, H.; Lv, C. A review of estimation for vehicle tire-road interactions toward automated driving. *IEEE Trans. Syst. Man Cybern. Syst.* **2018**, *49*, 14–30. [\[CrossRef\]](#)
- Klomp, M.; Gao, Y.; Bruzelius, F. Longitudinal velocity and road slope estimation in hybrid electric vehicles employing early detection of excessive wheel slip. *Veh. Syst. Dyn.* **2014**, *52*, 172–188. [\[CrossRef\]](#)
- Mahyuddin, M.N.; Na, J.; Herrmann, G.; Ren, X.; Barber, P. Adaptive observer-based parameter estimation with application to road gradient and vehicle mass estimation. *IEEE Trans. Ind. Electron.* **2013**, *61*, 2851–2863. [\[CrossRef\]](#)
- Zhao, L.; Liu, Z. Vehicle velocity and roll angle estimation with road and friction adaptation for four-wheel independent drive electric vehicle. *Math. Probl. Eng.* **2014**, *2014*, 1–11. [\[CrossRef\]](#)
- Reina, G.; Messina, A. Vehicle dynamics estimation via augmented extended Kalman filtering. *Measurement* **2019**, *133*, 383–395. [\[CrossRef\]](#)
- Li, X.; Song, X.; Chan, C. Reliable vehicle sideslip angle fusion estimation using low-cost sensors. *Measurement* **2014**, *51*, 241–258. [\[CrossRef\]](#)
- Berntorp, K. Joint wheel-slip and vehicle-motion estimation based on inertial, GPS, and wheel-speed sensors. *IEEE Trans. Control Syst. Technol.* **2016**, *24*, 1020–1027. [\[CrossRef\]](#)
- Wenzel, T.A.; Burnham, K.J.; Blundell, M.V.; Williams, R.A. Dual extended Kalman filter for vehicle state and parameter estimation. *Veh. Syst. Dyn.* **2006**, *44*, 153–171. [\[CrossRef\]](#)
- McIntyre, M.L.; Ghotikar, T.J.; Vahidi, A.; Song, X.; Dawson, D.M. A two-stage Lyapunov-based estimator for estimation of vehicle mass and road grade. *IEEE Trans. Veh. Technol.* **2008**, *58*, 3177–3185. [\[CrossRef\]](#)
- Vahidi, A.; Stefanopoulou, A.; Peng, H. Recursive least squares with forgetting for online estimation of vehicle mass and road grade: theory and experiments. *Veh. Syst. Dyn.* **2005**, *43*, 31–55. [\[CrossRef\]](#)
- Sun, Y.; Li, L.; Yan, B.; Yang, C.; Tang, G. A hybrid algorithm combining EKF and RLS in synchronous estimation of road grade and vehicle' mass for a hybrid electric bus. *Mech. Syst. Signal Proc.* **2016**, *68*, 416–430. [\[CrossRef\]](#)
- Li, X.; Ma, J.; Zhao, X.; Wang, L. Intelligent Two-Step Estimation Approach for Vehicle Mass and Road Grade. *IEEE Access* **2020**, *8*, 218853–218862. [\[CrossRef\]](#)
- Kim, S.; Shin, K.; Yoo, C.; Huh, K. Development of algorithms for commercial vehicle mass and road grade estimation. *Int. J. Automot. Technol.* **2017**, *18*, 1077–1083. [\[CrossRef\]](#)
- Hong, S.; Lee, C.; Borrelli, F.; Hedrick, J.K. A novel approach for vehicle inertial parameter identification using a dual Kalman filter. *IEEE Trans. Intell. Transp. Syst.* **2014**, *16*, 151–161. [\[CrossRef\]](#)
- Wan, E.A.; Nelson, A.T. Dual extended Kalman filter methods. In *Kalman Filtering and Neural Networks*; Haykin, S., Ed.; Publishing House: New York, NY, USA, 2001; pp. 123–163.
- Chen, T.; Xu, X.; Chen, L.; Jiang, H.; Cai, Y.; Li, Y. Estimation of longitudinal force, lateral vehicle speed and yaw rate for four-wheel independent driven electric vehicles. *Mech. Syst. Signal Proc.* **2015**, *101*, 377–388. [\[CrossRef\]](#)
- Viehweger, M.; Vasseur, C.; Van Aalst, S.; Acosta, M.; Regolin, E.; Alatorre, A.; Desmet, W.; Naets, F.; Ivanov, V.; Ferrara, A. Vehicle state and tyre force estimation: demonstrations and guidelines. *Veh. Syst. Dyn.* **2020**, *6*, 1–28. [\[CrossRef\]](#)
- Park, G.; Choi, S.B. An Integrated Observer for Real-Time Estimation of Vehicle Center of Gravity Height. *IEEE Trans. Intell. Transp. Syst.* **2020**, *99*, 1–12. [\[CrossRef\]](#)
- Marzbanrad, J.; Tahbaz-zadeh Moghaddam, I. Self-tuning control algorithm design for vehicle adaptive cruise control system through real-time estimation of vehicle parameters and road grade. *Veh. Syst. Dyn.* **2016**, *54*, 1291–1316. [\[CrossRef\]](#)
- Berntorp, K.; Di Cairano, S. Tire-stiffness and vehicle-state estimation based on noise-adaptive particle filtering. *IEEE Trans. Control Syst. Technol.* **2019**, *27*, 1100–1114. [\[CrossRef\]](#)

21. Saeed, T.U. Road Infrastructure Readiness for Autonomous Vehicles. Ph.D. Thesis, Purdue University Graduate School, West Lafayette, Indiana, 2019.
22. Volovski, M.; Murillo-Hoyos, J.; Saeed, T.U.; Labi, S. Estimation of routine maintenance expenditures for highway pavement segments: accounting for heterogeneity using random-effects models. *J. Transp. Eng. A Syst.* **2017**, *5*, 4017006. [[CrossRef](#)]
23. Mannering, F.L.; Shankar, V.; Bhat, C.R. Unobserved heterogeneity and the statistical analysis of highway accident data. *Anal. Methods Accid. R.* **2016**, *11*, 1–16. [[CrossRef](#)]
24. Saeed, T.U.; Qiao, Y.; Chen, S.; Gkritza, K.; Labi, S. Methodology for probabilistic modeling of highway bridge infrastructure condition: Accounting for improvement effectiveness and incorporating random effects. *J. Infrastruct. Syst.* **2017**, *23*, 4017030. [[CrossRef](#)]
25. Waseem, M.; Ahmed, A.; Saeed, T.U. Factors affecting motorcyclists' injury severities: An empirical assessment using random parameters logit model with heterogeneity in means and variances. *Accid. Anal. Prev.* **2019**, *123*, 12–19. [[CrossRef](#)] [[PubMed](#)]
26. Saeed, T.U.; Burris, M.W.; Labi, S.; Sinha, K.C. An empirical discourse on forecasting the use of autonomous vehicles using consumers' preferences. *Technol. Forecast. Soc. Chang.* **2020**, *158*, 120130. [[CrossRef](#)]
27. Yamany, M.S.; Saeed, T.U.; Volovski, M.; Ahmed, A. Characterizing the performance of interstate flexible pavements using artificial neural networks and random parameters regression. *J. Infrastruct. Syst.* **2020**, *26*, 4020010. [[CrossRef](#)]
28. Dugoff, H.; Fancher, P.S.; Segel, L. An analysis of tire traction properties and their influence on vehicle dynamic performance. *SAE Trans.* **1970**, *79*, 1219–1243.
29. Arasaratnam, I.; Haykin, S. Cubature Kalman filters. *IEEE Trans. Autom. Control* **2009**, *54*, 1254–1269. [[CrossRef](#)]
30. Huang, Y.; Zhang, Y.; Wu, Z.; Li, N.; Chambers, J. A novel adaptive Kalman filter with inaccurate process and measurement noise covariance matrices. *IEEE Trans. Autom. Control* **2018**, *63*, 594–601. [[CrossRef](#)]
31. Xiao, Z.; Xiao, D.; Havyarimana, V.; Jiang, H.; Liu, D.; Wang, D.; Zeng, F. Toward accurate vehicle state estimation under non-gaussian noises. *IEEE Internet Things J.* **2019**, *6*, 10652–10664. [[CrossRef](#)]
32. O'Hagan, A.; Forster, J.J. *Kendall's Advanced Theory of Statistics, Volume 2B: Bayesian Inference*, 2nd ed.; Arnold: London, UK, 2004.
33. Lin, N.; Shi, S. Road grade estimation based on the curvature of the vertical profile of a road. *Proc. Inst. Mech. Eng. Part D J. Automob. Eng.* **2016**, *231*, 476–486. [[CrossRef](#)]
34. Li, B.; Zhang, J.; Du, H.; Li, W. Two-layer structure based adaptive estimation for vehicle mass and road slope under longitudinal motion. *Measurement* **2017**, *95*, 439–455. [[CrossRef](#)]
35. Luenberger, D. An introduction to observers. *IEEE Trans. Autom. Control* **1971**, *16*, 596–602. [[CrossRef](#)]
36. Share Pasand, M.M. Cubic observers for a class of nonlinear systems with input and output delays. *arXiv* **2019**, arXiv:1912.10394.
37. Share Pasand, M.M. Luenberger-type cubic observers for state estimation of linear systems. *Int. J. Adapt. Control Signal Process.* **2020**, *34*, 1148–1161. [[CrossRef](#)]